Received 24 December 1998; accepted 17 May 1999.

1. Miyata, H. & Miyata, M. Mode of conjugation in homothallic cells of *Schizosaccharomyces pombe*. *J. Gen. Appl. Microbiol.* **27,** 365–371 (1981).
2. Egel, R. & Eie, B. Cell lineage asymmetry in *Schizosaccharomyces pombe*: unilateral transmission of a high-frequency state of mating-type switching in diploid pedigrees. *Curr. Genet.* **12,** 429–433 (1987).
3. Klar, A. J. S. Differentiated parental DNA strands confer developmental asymmetry on daughter cells in fission yeast. *Nature* **326,** 466–470 (1987).
4. Klar, A. J. S. The developmental fate of fission yeast cells is determined by the pattern of inheritance of parental and grandparental DNA strands. *EMBO J.* **9,** 1407–1415 (1990).
5. Klar, A. J. S. & Bonaduce, M. J. The mechanism of fission yeast mating-type interconversion: evidence for two types of epigenetically inherited chromosomal imprinted events. *Cold Spring Harb. Symp. Quant. Biol.* **58,** 457–465 (1993).
6. Beach, D. H. Cell type switching by DNA transposition in fission yeast. *Nature* **305,** 682–687 (1983).
7. Nielsen, O. & Egel, R. Mapping the double-strand breaks at the mating-type locus in fission yeast by genomic sequencing. *EMBO J.* **8,** 269–276 (1989).
8. Klar, A. J. S. & Miglio, L. M. Initiation of meiotic recombination by double-strand DNA breaks in *S. pombe*. *Cell* **46,** 725–731 (1986).
9. Moreno, S. A., Klar, A. J. S. & Nurse, P. Molecular genetic analysis of fission yeast *Schizosaccharomyces pombe*. *Methods Enzymol.* **194,** 795–823 (1991).
10. Egel, R., Beach, D. H. & Klar, A. J. S. Genes required for initiation and resolution steps of mating-type switching in fission yeast. *Proc. Natl Acad. Sci. USA* **81,** 3481–3485 (1984).
11. Singh, J. & Klar, A. J. S. DNA polymerase-α is essential for mating-type switching in fission yeast. *Nature* **361,** 271–273 (1993).
12. Caddle, M. S. & Calos, M. P. Specific initiation at an origin of replication from *Schizosaccharomyces pombe*. *Mol. Cell. Biol.* **14,** 1796–1805 (1994).
13. Clyne, R. K. & Kelly, T. J. Genetic analysis of an ARS element from the fission yeast *Schizosaccharomyces pombe*. *EMBO J.* **14,** 6348–6357 (1995).
14. Brewer, B. J., Lockshon, D. & Fangman, W. L. The arrest of replication forks in the rDNA of yeast occurs independently of transcription. *Cell* **71,** 267–276 (1992).
15. Arcangioli, B. A site- and strand-specific DNA break confers asymmetric switching potential in fission yeast. *EMBO J.* **17,** 4503–4510 (1998).
16. Klar, A. J. S. Lineage-dependent mating-type transposition in fission and budding yeast. *Curr. Opin. Genet. Dev.* **3,** 745–751 (1993).
17. Sambrook, J., Fritsch, E. F. & Maniatis, T. *Molecular Cloning: A Laboratory Manual* 2nd ed (Cold Spring Harbor Laboratory Press, New York, 1989).
18. MacDonell, M. W., Simon, M. W. & Studier, F. W. Analysis of restriction fragments of T7 DNA and determination of molecular weights by electrophoresis in neutral and alkaline gels. *J. Mol. Biol.* **110,** 119–146 (1977).
19. Egel, R. in *Molecular Biology of the Fission Yeast* (eds Nasim, A., Young, P. & Johnson, B. F.) 31–74 (Academic, San Diego, 1989).
20. Klar, A. J. S., Ivanova, A. V., Dalgaard, J. Z., Bonaduce, M. J. & Grewal, S. I. S. in *Epigenetics* (ed. Cardew, G.) 87–103 (Novartis Foundation Symposium 214, Wiley, Chichester, 1998).
21. Arcangioli, B. & Klar, A. J. S. A novel switch-activating site (SAS1) and its cognate binding factor (SAP1) required for efficient *mat1* switching in *Schizosaccharomyces pombe*. *EMBO J.* **10,** 3025–3032 (1991).
22. Styrkarsdottir, U., Egel, R. & Nielsen, O. The smt-0 mutation which abolishes mating-type switching in fission yeast is a deletion. *Curr. Genet.* **23,** 184–186 (1993).
23. Gerring, S. L., Connelly, C. & Hieter, P. in *Guide to Yeast Genetics and Molecular Biology* (eds Fink, G. & Guthrie, C.) 57–76 (Academic, San Diego, 1991).
24. Bresch, C., Muller, G. & Egel, R. Genes involved in meiosis and sporulation of a yeast. *Mol. Gen. Genet.* **102,** 301–306 (1968).

Acknowledgements. We thank our colleagues at ABL for suggestions and helpful discussions; B. Brewer, M. Hoant and S. Hunt for help with the analysis of replication intermediates; A. Arthur for editorial suggestions; and R. Frederickson for the art work. This work was sponsored by the Danish Natural Science Research Council (J.Z.D.) and the National Cancer Institute, Department of Health and Human Services, under contract with ABL. The contents of this article do not necessarily reflect the views or politics of the DHHS, nor does mention of trade names, commercial products, or organizations imply endorsement by the US Government.

Correspondence and requests for materials should be addressed to A.K. (e-mail: klar@mail.ncifcrf.gov).

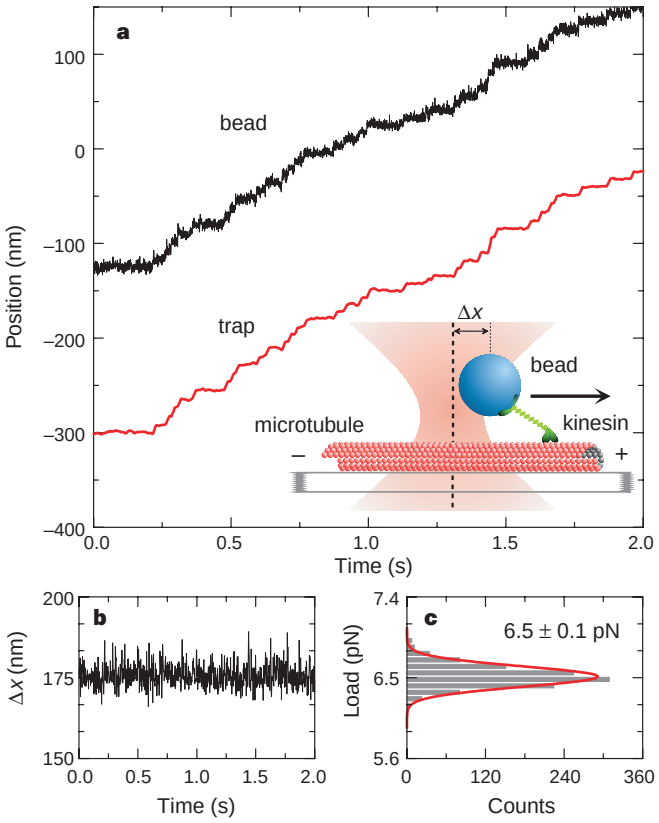

Figure 1 Operation of the force clamp. **a**, Sample record from the force clamp, showing kinesin-driven bead movement and corresponding optical trap displacement (2 mM ATP). Discrete steps of 8 nm are readily apparent. Inset, schematic representation of the motility assay used, showing the experimental geometry (not to scale). The separation between bead and trap was nominally fixed at $\Delta x = 175$ nm. Bead position was sampled at 20 kHz, filtered with a 12-ms boxcar window for the feedback on the trap deflection, and saved unfiltered at 2.0 kHz. **b**, The measured bead–trap separation, Δx, for the record in **a**. **c**, Histogram of the displacements in **b**, converted to force by multiplying by the trap stiffness (0.037 pN nm^{-1}). Solid red line is gaussian fit to these data, yielding a load of 6.5 ± 0.1 pN (mean ± s.d.).

Single kinesin molecules studied with a molecular force clamp

Koen Visscher*†‡, Mark J. Schnitzer*§‡ & Steven M. Block*†§

* *Department of Molecular Biology,* † *Princeton Materials Institute, and*
§ *Department of Physics, Princeton University, Princeton, New Jersey 08544, USA*
‡ *These authors contributed equally to this work.*

Kinesin is a two-headed, ATP-driven motor protein that moves processively along microtubules in discrete steps of 8 nm, probably by advancing each of its heads alternately in sequence[1–4]. Molecular details of how the chemical energy stored in ATP is coupled to mechanical displacement remain obscure. To shed light on this question, a force clamp was constructed, based on a feedback-driven optical trap capable of maintaining constant loads on single kinesin motors[5]. The instrument provides unprecedented resolution of molecular motion and permits mechanochemical studies under controlled external loads. Analysis of records of kinesin motion under variable ATP concentrations and loads revealed several new features. First, kinesin stepping appears to be tightly coupled to ATP hydrolysis over a wide range of forces, with a single hydrolysis per 8-nm mechanical advance. Second, the kinesin stall force depends on the ATP concentration. Third, increased loads reduce the maximum velocity as expected, but also raise the apparent Michaelis–Menten constant. The kinesin cycle therefore contains at least one load-dependent transition affecting the rate at which ATP molecules bind and subsequently commit to hydrolysis. It is likely that at least one other load-dependent rate exists, affecting turnover number. Together, these findings will necessitate revisions to our understanding of how kinesin motors function.

The mechanochemical coupling ratio relates the number of ATP molecules hydrolysed to the distance travelled during a single enzymatic cycle. Determination of this ratio over a range of loads sheds light on the mechanism for movement, and has been considered one of the most pressing challenges in the motility field[1]. However, for the microtubule-based molecular motor kinesin, the task is by no means straightforward. Direct comparisons between solution ATPase measurements and motility *in vitro* are only feasible in the absence of external loads, as these cannot be applied in bulk solution. Single-molecule fluorescence methods,

which have been used to correlate motor movement with nucleotide binding and release in the actomyosin system[6,7], have proved difficult to realize with kinesin because it has a lower affinity for ATP: concentrations of fluorescent ATP analogues sparse enough to detect as single fluorophores yield negligible rates of movement. Coupling ratios may also be inferred from an analysis of fluctuations in displacement records of single molecules, but this approach requires continuous records over comparatively large distances under invariant loads[8,9]. Such records are hard to obtain using either conventional laser-based optical traps[10–12] or microneedles[13], where loads change continually as motors progress.

We solved the latter difficulty by developing an optical force clamp that can record displacements of single kinesin molecules over hundreds of nanometres while maintaining the average load to within a fraction of a piconewton[5] (Fig. 1). In the assay, a kinesin molecule adsorbed to a silica bead (0.5 μm in diameter) moves processively along an immobilized microtubule[3] while an optical trap follows its motion (Fig. 1a). Bead movement is monitored with subnanometre resolution by a quadrant photodiode, which detects scattered light from a fibre-coupled HeNe laser source[14]. Because force on the bead is proportional to its displacement from the trap centre[15], load can be maintained by a servo system that dynamically adjusts this separation to some preset value, using digital feedback to control acousto-optical deflectors which move the trap position as required (Fig. 1b, c). In contrast to other feedback-enhanced optical traps developed for isometric force measurements[16–18], a force clamp is particularly suited to isotonic displacement measurements[5]. A further benefit of a force clamp is that, unlike other optical trapping systems, displacement data do not require corrections for the series elastic compliance between the bead and motor, hitherto a source of experimental uncertainty amounting to 20% or more[3,5]. Force clamps therefore provide exceptionally clear molecular records, and individual 8-nm steps can be readily visualized at kilohertz bandwidths, even for high ATP levels (Fig. 1a).

We first used this system to study kinesin velocity as a function of ATP concentration at fixed load. For negligible loads, the velocity, v, obeys Michaelis–Menten kinetics, $v = V_{max}[ATP]/([ATP] + K_m)$, in both microtubule gliding[4] and bead-based[8,9] assays. The maximum velocity at saturating ATP levels, V_{max}, is expected to fall with increased load, but how will the apparent Michaelis–Menten constant, K_m, change—if at all? Alternative coupling schemes supply different predictions. Simple loosely coupled models[10] postulate a maximum hydrolysis rate, k_{cat}, that is independent of the applied force, F, with a load-dependent coupling efficiency, $\epsilon(F)$, between ATP hydrolysis and mechanical stepping (with $V_{max} = \epsilon(F)dk_{cat}$; $d = 8$ nm). In practice, the coupling ratio has been shown to be independent of ATP concentration and 1:1 at negligible loads[8,9]; that is, there is one hydrolysis for every 8 nm advance. Because neither k_{cat} nor k_b, the effective rate of ATP binding (defined as $k_b = k_{cat}/K_m$), depends on load in these models, it follows that $K_m = k_{cat}/k_b$ must be load-invariant[10,19]. In contrast, simple tightly coupled models incorporate a single mechanically sensitive rate that affects k_{cat} but leaves ϵ and k_b unchanged. Under increased load, k_{cat} slows, reducing both K_m and V_{max}.

Experimentally, high loads reduced V_{max} as anticipated. Surprisingly, however, they also raised K_m (Fig. 2), a phenomenon that is inconsistent with either simple model. At the lowest load tested (1.05 ± 0.01 pN), V_{max} was 813 ± 28 nm s^{-1} and K_m was 88 ± 7 μM, comparable to values obtained previously for negligible loads[4,8,9]. At moderate loads (3.59 ± 0.03 pN), V_{max} dropped to 715 ± 19 nm s^{-1} while K_m rose to 140 ± 6 μM. At the highest load tested (5.63 ± 0.06 pN), V_{max} dropped further to 404 ± 32 nm s^{-1}, while K_m rose to 312 ± 49 μM. Because $K_m = k_{cat}/k_b$, any increase in K_m—given the drop in V_{max}—implies that k_b decreases substantially with increased load. Thus, the application of load has two important effects on the kinesin cycle: it lowers the maximal stepping rate, and it also lowers the effective rate of ATP binding.

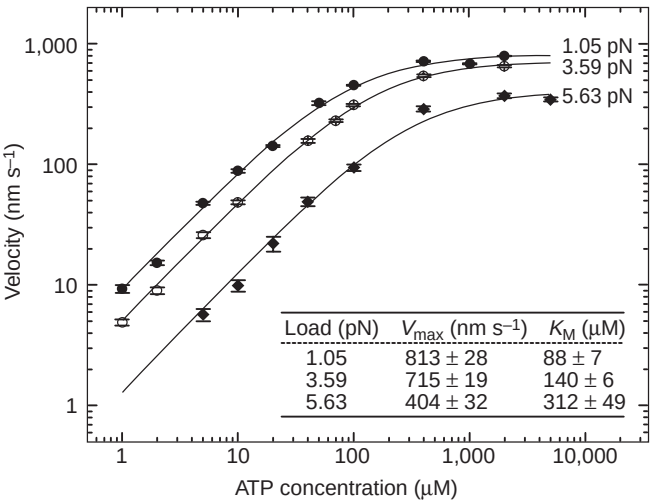

Figure 2 Michaelis–Menten kinetics under load. Double logarithmic plot of the average bead velocity, v (mean ± s.e.m.), versus ATP concentration for various loads (filled circles, 1.05 ± 0.01 pN, N = 11–102 runs; open circles, 3.59 ± 0.03 pN, N = 8–79 runs; diamonds, 5.63 ± 0.06 pN, N = 19–58 runs). Data were fitted to Michaelis–Menten curves (lines), $v = V_{max}[ATP]/([ATP] + K_m)$. Inset, fit parameters, V_{max} and K_m.

What causes the effective binding rate to decline under load? For a generalized ATPase pathway involving N intermediate states

$$1 \underset{k_{off}}{\overset{k_{on}[ATP]}{\longleftrightarrow}} 2 \underset{k_{-2}}{\overset{k_2}{\longleftrightarrow}} 3 \underset{k_{-3}}{\overset{k_3}{\longleftrightarrow}} \cdots \rightarrow \cdots N \underset{k_{-N}}{\overset{k_N}{\longleftrightarrow}} 1$$

there are at least three possible mechanisms. The first is that k_b falls because the second-order ATP binding rate, k_{on}, is reduced by load. The second is that k_b falls because of an increase in the ATP unbinding rate, k_{off}. In either event, the observed drop in V_{max} must arise from some other transition because, for pathways with an irreversible step, such as the kinesin cycle[20], neither k_{on} nor k_{off} affects either k_{cat} or ϵ. The third possible mechanism is somewhat more subtle, and involves a reduction in the rate following binding, k_2. When k_2 falls, the ATP affinity (k_{on}/k_{off}) is unaffected, but a greater fraction of ATP molecules will unbind before hydrolysis, reducing the effective binding rate (the rate at which ATP molecules are committed to the remainder of the hydrolysis pathway). Because k_2 also affects k_{cat}, lowering k_2 alone could reduce k_{cat} and raise K_m simultaneously, but only if k_{off} were sufficiently fast. (More generally, a change in one or more reversible transitions subsequent to ATP binding but before the first irreversible transition could produce a similar effect, given sufficiently fast reverse rates.) The nearly fourfold increase found for K_m accompanying a drop in speed by a factor of two would require a k_{off} of not less than 650 s^{-1}, which is significantly faster than ATP unbinding rates of 50–200 s^{-1} reported in solution studies[21,22]. However, the latter estimates were determined indirectly and were subject to simplifying assumptions, so their experimental uncertainties remain fairly large. A k_2-based mechanism therefore ought not be excluded solely on this basis. Notwithstanding, the interpretation we favour is that the contrary behaviour of V_{max} and K_m derives from two independent, mechanically sensitive rates, one of which affects ATP binding through k_{on} and/or k_{off}.

Regardless of the candidate mechanism, the two effects of load on the mechanochemical pathway imply that kinesin force–velocity curves should display different shapes for different ATP concentrations. However, this inference appears to be at odds with several previous studies of force and velocity using either fixed optical

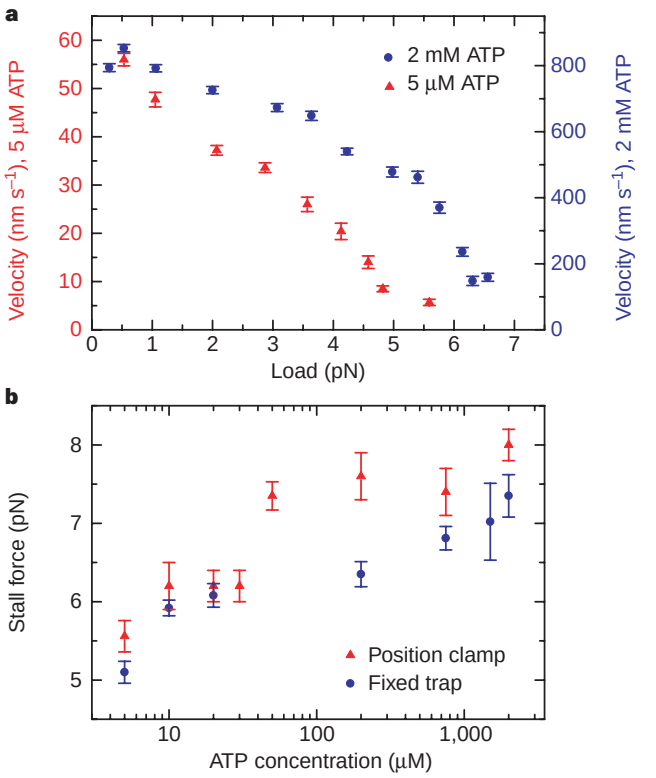

Figure 3 Load dependence of motility. **a**, Average bead velocity, v (mean ± s.e.m.), versus applied load for fixed ATP concentrations (red triangles, left axis, 5 μM ATP, N = 19–57; blue circles, right axis, 2 mM ATP, N = 37–87). The velocity point at (5.6 pN, 5 μM ATP) is likely to represent an overestimate because beads which stalled completely (v = 0) were indistinguishable from beads lacking active motors, and so were not included in the analysis. **b**, Stall force (mean ± s.e.m.) versus ATP concentration, measured either with the position clamp[17,18] (red triangles) or with a fixed optical trap (blue circles). Stalls had to last a minimum of 2 s to be included in the analysis. Data points represent an average of either 12–29 (position clamp) or 6–70 (fixed trap) stalls.

traps[10–12] or microneedles[13], all of which reported nearly linear decreases in velocity with increased load, for both limiting and saturating ATP concentrations. In fact, such linear force–velocity relations formed the basis of an argument for a load-independent K_m (refs 10, 19) which supported a simple, loosely coupled picture[10]. However, the earlier studies lacked the improved resolution afforded by the force clamp, and subtle differences in shape were not distinguished within experimental error. Data from all previous studies consistently showed a lower stall force at limiting ATP than at saturating ATP, although the difference in force was insufficient in any given experiment to have been considered significant. Moreover, a greater discrepancy (~1 pN) between the stall force at limiting and saturating ATP was observed when the limiting concentration of ATP was ~35-fold lower than the unloaded K_m (ref. 13), as compared to when limiting ATP values were only ~6-fold lower (~0.5 pN, refs 10–12). We therefore measured velocity as a function of load in the force clamp at both 2 mM and 5 μM ATP, choosing the lower ATP level to be >17-fold below the unloaded K_m to highlight any potential differences.

Force–velocity curves obtained with the force clamp displayed different shapes at limiting and saturating ATP levels (Fig. 3a), and they also showed different stall forces. The 5-μM curve is nearly linear, with a stall force of ~5.5 pN. In contrast, the 2-mM curve is concave down, and supports a greater stall force of ~7.0 pN. Strikingly, a 5-pN load leads to a ~40% decline in speed for 2 mM ATP, whereas at 5 μM ATP an identical load is sufficient to halt movement almost entirely. These results are consistent with a role for load in lowering the effective rate of ATP binding. At limiting ATP, k_b becomes much lower than k_{cat}, and therefore the stall force becomes independent of the latter. However, at 2 mM ATP, the stall force probably depends on both k_b and k_{cat}, as K_m rises beyond ~300 μM at loads of 7 pN or more. Although the stall force may depend on additional factors at all ATP levels, stall forces are expected to rise continuously from ~5.5 pN to ~7.0 pN as the ATP concentration is raised.

To further test this supposition, we measured the ATP dependence of kinesin stall force by two additional methods, using either an optical position clamp or a fixed trap. The position clamp[17], based on an optical trapping interferometer, is well suited to isometric measurements of stall force[16], and was used previously to study force generation by individual RNA polymerase molecules[18]. Position clamp measurements on single kinesin motors gave stall forces that rose with ATP concentration, as anticipated (Fig. 3b). An inherent problem encountered in these experiments was the dramatic decline in kinesin processivity at loads approaching stall[12]. Rapid detachment of beads from the microtubule made the collection of a large data set prohibitive, and accounted for much of the experimental scatter (Fig. 3b). To confirm the position clamp measurements, we also measured stall forces using a fixed optical trap. Kinesin-coated beads moving outwards in a stationary trap experience increasing loads until they arrive at a position where forward progress ceases: the final displacement, multiplied by the trap stiffness, supplies a measure of the stall force[12]. Kinesin stall forces determined by this method exhibit a similar increase with ATP concentration (Fig. 3b).

How is the kinesin ATPase pathway coupled to mechanical movement under load? One possibility is that kinesin coupling is tight, involving no futile hydrolysis events that fail to generate movement, even under load (that is, $\epsilon = 1$). In this case, any changes in the rates of load-dependent transitions must account entirely for the observed decreases in velocity under load. However, more complicated scenarios may be entertained. Although the rise in K_m with load eliminates the simpler versions of loose coupling, mechanochemical coupling in kinesin might display an admixture of both tight and loose elements, with load-dependent transitions and unproductive hydrolyses conspiring jointly to lower the velocity. Another candidate mechanism for loose coupling involves an increase in the frequency of 8-nm backwards steps[10–12] with load. However, the latter mechanism may be discounted because the fraction of backwards steps found in this study (data not shown) and by others remains only ~5–10% at both negligible[8,11] and substantial[11,12] loads.

To study the coupling mechanism under load, we performed a fluctuation analysis[23,24] of kinesin movement subjected to the force clamp. Fluctuation analysis, which relies on the processive property exhibited by some molecular motors, has been used previously to study ATP coupling in kinesin near zero load[8], as well as the duty ratio of the bacterial rotary motor under torque[25]. Fluctuations in displacement are quantified by a randomness parameter, r, which measures the temporal irregularity of mechanical advances. For an ensemble of displacement records, $x(t)$, r is defined by

$$r = \lim_{t\to\infty} \frac{\langle x^2(t)\rangle - \langle x(t)\rangle^2}{d\langle x(t)\rangle}$$

where d is the motor step size, and the angle brackets denote an ensemble average[23,24]. A perfectly clocklike motor displays no stepping irregularity, and has $r = 0$, whereas a 'Poisson' motor with one biochemical transition moves at exponentially distributed intervals, and has $r = 1$. In general, r^{-1} provides a continuous measure of the number of rate-limiting transitions in the overall mechanochemical cycle. Determinations of randomness are insensitive to thermal or other stationary noise and can therefore be performed even when individual steps are not resolved. When steps can be discerned amid

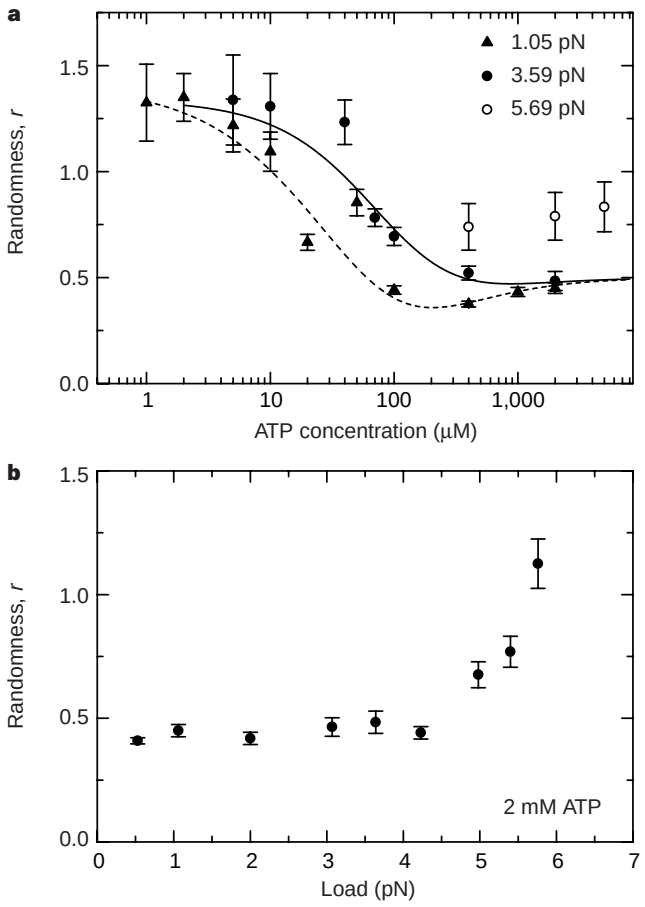

Figure 4 Displacement fluctuations. **a**, Semi-logarithmic plot of the randomness parameter, r (mean ± s.e.m.), versus ATP concentration for fixed loads (filled triangles, 1.05 pN ± 0.01, $N = 11$–102; filled circles, 3.59 ± 0.03 pN, $N = 30$–79; open circles, 5.69 ± 0.03 pN). The rise in r from $\sim\frac{1}{2}$ to ~1 begins at a higher ATP level for 3.59 pN than for 1.05 pN, reflecting the higher K_m at the former load. To guide the eye, data are compared to two-parameter analytical fits (dashed line, 1.05 pN; solid line, 3.59 pN). These fits were performed using the Michaelis–Menten parameters from Fig. 2, assuming two rate-limiting transitions at saturating ATP and one ATP hydrolysis per 8-nm step. Backward steps were assumed to occur in an ATP-dependent manner (see Methods). **b**, The randomness parameter, r (mean ± s.e.m.), versus load at 2 mM ATP (circles). Data points represent an average of 43–87 runs.

noise, fluctuation analysis is more robust than a direct analysis of stepping intervals, which suffers from the 'missing event' problem[23], an inability to distinguish the shortest steps. However, r is affected by phenomena that increase fluctuations at long time scales, such as backwards steps, enzyme inactivations, or futile hydrolyses. All of these can raise r, sometimes beyond unity[8,23].

The determination of r for negligible loads at limiting ATP verified that mechanochemical coupling was 1:1 in this regime[8]. Moreover, for minimal loads and saturating ATP, r was $\sim\frac{1}{2}$, which is indicative of two ATP-independent, rate-limiting transitions per step[8,23]. But how is the randomness affected by the application of an external load? In the 'tightly coupled' scenario, the coupling is load-invariant by definition, so the ATP dependence of r must be correspondingly invariant, at least out to forces where there are still about two rate-limiting transitions. Tight coupling therefore predicts $r \approx \frac{1}{2}$ at saturating ATP, independent of load. In sharp contrast, 'loosely coupled' scenarios that invoke a decrease in coupling efficiency[10] lead to a randomness that rises with load, in proportion to the concomitant decrease in velocity[23]. For such mechanisms, values for r at saturating ATP should rise upwards from $\frac{1}{2}$ towards 1 as load increases. Other 'loosely coupled' scenarios, such as those involving an increase in the frequency of backwards steps, should cause r to rise still more sharply. Coupling behaviour can therefore be studied by determining r as a function of load at saturating ATP levels. Nevertheless, at sufficiently high loads, even nominally tightly coupled schemes may lead to $r \approx 1$ at saturating ATP: this occurs for such high loads that the possibility for two rate-limiting transitions ultimately breaks down, as one or the other mechanically sensitive rate slows to become the sole determinant of velocity. At these extreme loads and beyond, one cannot distinguish between coupling mechanisms through measurements of randomness.

Measurements of the ATP dependence of randomness for low external load (1.05 ± 0.01 pN; Fig. 4) were similar to those obtained near zero load[8]: r rose from $\sim\frac{1}{2}$ at saturating ATP through 1 when ATP levels dropped below K_m (the increase in r above unity probably reflects the occurrence of 8-nm backwards steps, comprising 5–10% of all steps[8,11,12], as discussed[8]). A similar dependence of r upon ATP concentration was observed for a fixed load of 3.59 ± 0.03 pN (equal to about half the stall force), an observation that is consistent with tight coupling. Still stronger evidence in support of tight coupling came from the determination of randomness as a function of load for saturating ATP levels. The data of Fig. 4b show r to be nearly independent of load out to forces approaching ~5 pN: this invariance constitutes a clear signature of tight coupling, and can be used to place a theoretical bound on the fraction of total ATP hydrolyses that fail to produce movement. Even in conservative scenarios involving only 3% or 4% backwards steps, to remain consistent with these data the fraction of futile hydrolyses must be less than 15% or 10%, respectively, of all events. More realistic frequencies of backward stepping which are slightly higher[8,11,12] lead to an even lower bound. (It is nevertheless possible to construct more complicated reaction schemes involving ~1–2% backwards steps, plus more than four rate-limiting biochemical transitions under load, which admit a larger fraction of unproductive hydrolyses. However, we are inclined to exclude such complexities because they seem inconsistent with motility[8,23,24] and solution[21,22] studies suggesting that kinesin's microtubule-stimulated ATPase has only about two rate-limiting transitions in the absence of load.) For forces approaching stall (beyond 5 pN; Fig. 4b), r rises steeply through 1, and these data alone do not indicate whether coupling remains tight. However, at 5.69 pN, we found no significant difference between r at 2 mM ATP and at an ATP level comparable to K_m (400 μM; Fig. 4a), an observation consistent with a rise in futile hydrolyses at extreme loads. Because of the loss of processivity, however, we were unable to measure r for 5.69 pN at more than a few ATP levels (Fig. 4a). *In vivo*, detachment may serve to prevent kinesin motors from wasting ATP when faced with insurmountable loads[2].

The finding of tight coupling between ATP hydrolysis and mechanical stepping would seem to rule out many current theoretical models for force generation by kinesin. One class of models that is inconsistent with our findings predicts that most of the velocity decline under load is due to a loss of coupling efficiency and incorporates either pure loose coupling[10], or at most one force-sensitive transition[26–29]. Another apparently untenable class of models constitutes the so-called thermal ratchets (reviewed in ref. 30), for which the coupling efficiency depends sharply on load. However, we believe that the energy landscape picture proposed to explain the motion of RNA polymerase[18] might be adapted to accommodate kinesin mechanochemistry.

Additional experimental work lends support to our conclusions. Recent studies of the average kinesin displacement under load following the release of caged ATP appear to be consistent with tight coupling[31]. Moreover, earlier experiments that tested the application of loads in the same direction as kinesin motion demonstrated an increase in velocity for both limiting and high

ATP levels[12]. This counterintuitive finding may be explained by assuming that kinesin has two load-dependent transitions. The application of forward loads would raise the rates of both load-dependent transitions, leading to velocity increases when k_b is limiting at low ATP, but also when k_{cat} is limiting at high ATP.

Which transitions in the kinesin mechanical cycle are load-dependent? If load affects two (or more) biochemical transitions, one possibility is that each 8-nm kinesin mechanical step might comprise two shorter 'substeps' (ref. 32). However, although substeps represent transitions that seem likely to be load-dependent, they may lack the requisite ATP dependence, or they might be rapid and not rate-limiting even under load. Therefore, possible substeps in the 8-nm advance need not represent two load-dependent transitions. Conversely, a finding of two load-dependent transitions does not imply the existence of substeps: these transitions might correspond to biochemical events distinct from those which actually produce the forward progress, for example ATP binding and/or ADP release. Finally, because kinesin molecules carry two heads which are thought to operate 'hand over hand' in alternation, it remains an open question as to whether two load-dependent transitions take place within the same head or are instead shared between them. Further experiments will be required to determine the number and location of load-dependent transitions within the kinesin mechanochemical cycle. □

Methods

Assays. Motility assays were performed as described[8]. All chemicals were from Sigma, except glucose oxidase (250 μg ml^{-1}) and catalase (30 μg ml^{-1}), which were from Calbiochem.

Instrumentation and calibration. In brief, the optical trap was based on a Diaphot 200 inverted microscope (Nikon) outfitted to accommodate a 100×/1.3 NA oil-immersion objective (Plan-Neofluar, Zeiss), into which a Nd:YVO_4 laser beam (Spectra Physics; 1,064 nm) was introduced through a custom laser port (Nikon). Trap position within the specimen plane was specified using two acousto-optical deflectors (IntraAction) digitally controlled by computer. Position detection was accomplished by focusing a low-power (~400 μW HeNe laser beam (Uniphase, 633 nm, fibre-coupled) onto an optically trapped 0.5 μm silica bead and measuring the deflected light in a plane conjugate to the back focal plane of the microscope condenser using a quadrant photodiode arrangement[14]. The trapping laser and detector beam foci were coaligned both axially and laterally, so that both video-based centroid tracking of a bead and photodiode-based detection of its position produced the same velocities and displacements as measured from the trap centre. This alignment was done using kinesin-coated beads attached to microtubules by 2 mM AMP-PNP, a non-hydrolysable ATP analogue. To simulate motility, the piezoelectric microscope stage was moved in either a triangle wave or a stochastic stepping pattern while the bead was held in the force clamp. The position detector was calibrated each time a bead was selected or the position in the field of view had changed[14]. Trap stiffness calibrations[10,15] were done beforehand by determining the roll-off frequency of displacement power spectra for trapped beads as a function of laser power. To minimize differences in force arising from variation in the sizes of beads, we used a highly uniform population of silica spheres[10] (gift from E. Matijevic). The standard deviation in trap stiffness (and therefore the force at a given displacement) from bead to bead was 4.2% ($n = 100$), based on measured power spectra obtained from 10 individual beads at each of 10 different laser light levels. Linearity of the trap force for displacements out to 200 nm from the trap centre was verified by applying a sinusoidal displacement to the microscope stage and recording the response of a trapped bead[15].

To ensure accurate determinations of r, we performed control experiments analogous to those reported previously[8]. Kinesin-coated beads were placed on immobilized microtubules and motor activity was halted with AMP-PNP. To simulate single kinesin motion, the piezoelectric microscope stage was moved in discrete steps of 7–8 nm, at either fast (~660 nm s^{-1}) or slow (~14 nm s^{-1}) average speeds, at either high (~6 pN) or low (~1 pN) constant loads, and with stepping intervals chosen either from an exponential distribution ($r = 1$) or from a convolution of two exponentials ($r = \frac{1}{2}$). Under all eight possible conditions, control determinations of randomness and velocity were at worst within ~15% and ~5%, respectively, of their nominal values (data not shown). Before control and experimental runs, each bead was held ~300 nm above the microtubule and the position detector response was calibrated on-line[5,14]. To randomize measurement errors arising from vertical offsets, the microscope was refocused between runs such that the microtubule image was sharp when viewed by video-enhanced microscopy.

Records of bead displacements along microtubules that were aligned with a single axis (x) of the position detector were sampled at 19–21 kHz, anti-alias filtered at 10 kHz, digitized at 12-bit resolution, used for trap feedback, then decimated and saved to disk at 1.9–2.1 kHz. The force clamp thus operates along the x-axis only. The position of the optical trap was updated at 19–21 kHz but saved at 190–210 Hz for better computer performance. The running bead position was integrated with a variable (3–50 ms) boxcar window that was used to compute the updated trap position. We optimized the integration window during all control and experimental runs to improve feedback stability. Because the force clamp responds to variations in bead position averaged over the integration time, high-frequency force variations are permitted. To minimize variations caused by brownian motion of the bead, we set the bead-trap separation at 175 nm for all loads, except for the lowest loads of ~$\frac{1}{2}$ pN and ~1 pN, for which the separation was 100 nm to maintain a minimum trap stiffness. The load for each run was computed off-line from the known stiffness and the difference in the digitized bead and trap positions (Fig. 1). All runs used for analysis were required to lie laterally within ±50 nm of the microtubule axis. Upon activation of the feedback control program, a kinesin-coated bead was pulled to one edge of the detection zone, allowed to bind to the microtubule, and then to proceed towards the opposite edge of the zone: the load remained clamped over the interval (−150 nm, +150 nm) from the zone centre.

Stall force measurements using the position clamp were calibrated and performed as described[17]. In brief, position measurements were made with an optical trapping interferometer[3] distinct from the instrument used for the rest of this work, taking into account the slight variations in equilibrium bead position with laser power (these effects were calibrated before stall measurements were taken)[17]. Kinesin-driven beads were stalled at ~105 nm from the trap centre, and stalls were required to last >2 s to be scored. By multiplying this distance from the trap centre, the measured laser power at stall, and the predetermined trap stiffness (4.5×10^{-4} pN nm^{-1} mW^{-1}), stall forces were calculated. Stall force measurements using a fixed optical trap were done with the force-clamp instrument in its open-loop mode. Again, stalls were required to last for >2 s to be scored.

Analysis. Mean velocities, variance and randomness were determined using custom software written in LabView 5.0 (National Instruments) as described[8,23], except for the following. Experimental and control displacement records within ±150 nm of the detector centre were used. For inclusion in velocity analysis, runs had to last at least 100 nm (>5 pN) or 300 nm (<5 pN). Only runs over the full 300-nm range were used for the determination of r, except for the three r values at 5.69 ± 0.03 pN (Fig. 4a), for which we used runs of 150 nm minimum, because of the reduced processivity at high load. To determine the linear slope of the displacement variance versus time, a linefit was made to the variance over the first 40 nm/$\langle v \rangle$ time interval, excluding at least the first ~15 ms (the correlation time of the bead position in the force clamp). Experimental and control runs at limiting ATP levels were smoothed and resampled with a 10–25 ms window, a procedure that improves computational speed but does not affect r (ref. 8). To guide the eye, analytical fits to r versus ATP were made under the assumption of two rate-limiting transitions at saturating ATP and one ATP hydrolysis per 8-nm step[8]. To account for backwards steps, we fit to the formula[8] $r = (\tilde{r} - 1)(1 - 2P_-) + 1/1 - 2P_-$, where $\tilde{r}$ is the randomness in the absence of backwards steps, and P_-, the fraction of steps backwards, is inversely proportional to a linear function of [ATP].

Received 16 March; accepted 10 May 1999.

1. Howard, J. Molecular motors: structural adaptations to cellular functions. *Nature* **389,** 561–567 (1997).
2. Howard, J. The movement of kinesin along microtubules. *Annu. Rev. Physiol.* **58,** 703–729 (1996).
3. Svoboda, K., Schmidt, C. F., Schnapp, B. J. & Block, S. M. Direct observation of kinesin stepping by optical trapping interferometry. *Nature* **365,** 721–727 (1993).
4. Howard, J., Hudspeth, A. J. & Vale, R. D. Movement of microtubules by single kinesin molecules. *Nature* **342,** 154–158 (1989).

5. Visscher, K. & Block, S. M. Versatile optical traps with feedback control. *Methods Enzymol.* **298,** 460–489 (1998).
6. Funatsu, T., Harada, Y., Tokunaga, M., Saito, K. & Yanagida, T. Imaging of single fluorescent molecules and individual ATP turnovers by single myosin molecules in aqueous solution. *Nature* **374,** 555–559 (1995).
7. Ishijima, A. *et al*. Simultaneous observation of individual ATPase and mechanical events by a single myosin molecule during interaction with actin. *Cell* **92,** 161–171 (1998).
8. Schnitzer, M. J. & Block, S. M. Kinesin hydrolyses one ATP per 8-nm step. *Nature* **388,** 386–390 (1997).
9. Hua, W., Young, E. C., Fleming, M. L. & Gelles, J. Coupling of kinesin steps to ATP hydrolysis. *Nature* **388,** 390–393 (1997).
10. Svoboda, K. & Block, S. M. Force and velocity measured for single kinesin molecules. *Cell* **77,** 773–784 (1994).
11. Kojima, H., Muto, E., Higuchi, H. & Yanagida, T. Mechanics of single kinesin molecules measured by optical trapping nanometry. *Biophys. J.* **73,** 2012–2022 (1997).
12. Coppin, C. M., Pierce, D. W., Hsu, L. & Vale, R. D. The load dependence of kinesin's mechanical cycle. *Proc. Natl Acad. Sci. USA* **94,** 8539–8544 (1997).
13. Meyhöfer, E. & Howard, J. The force generated by a single kinesin molecule against an elastic load. *Proc. Natl Acad. Sci. USA* **92,** 574–578 (1995).
14. Visscher, K., Gross, S. P. & Block, S. M. Construction of multiple-beam optical traps with nanometer-resolution position sensing. *IEEE J. Sel. Topics Quantum. Electron.* **2,** 1066–1076 (1996).
15. Svoboda, K. & Block, S. M. Biological applications of optical forces. *Annu. Rev. Biophys. Biomol. Struct.* **23,** 247–285 (1994).
16. Finer, J. T., Simmons, R. M. & Spudich, J. A. Single myosin molecule mechanics: piconewton forces and nanometre steps. *Nature* **368,** 113–119 (1994).
17. Wang, M. D., Yin, H., Landick, R., Gelles, J. & Block, S. M. Stretching DNA with optical tweezers. *Biophys. J.* **72,** 1335–1346 (1996).
18. Wang, M. D. *et al*. Force and velocity measured for single molecules of RNA polymerase. *Science* **282,** 902–907 (1998).
19. Howard, J. The mechanics of force generation by kinesin. *Biophys. J.* **68,** 245s–255s (1995).
20. Hackney, D. Kinesin ATPase: Rate-limiting ADP release. *Proc. Natl Acad. Sci. USA* **85,** 6314–6318 (1988).
21. Gilbert, S. P., Webb, M. R., Brune, M. & Johnson, K. A. Pathway of processive ATP hydrolysis by kinesin. *Nature* **373,** 671–676 (1995).
22. Ma, Y. Z. & Taylor, E. W. Mechanism of microtubule kinesin ATPase. *Biochemistry* **34,** 13242–13251 (1995).
23. Svoboda, K., Mitra, P. P. & Block, S. M. Fluctuation analysis of motor protein movement and single enzyme kinetics. *Proc. Natl Acad. Sci. USA* **91,** 11782–11786 (1994).
24. Schnitzer, M. J. & Block, S. M. Statistical kinetics of processive enzymes. *Cold Spring Harbor Symp. Quant. Biol.* **60,** 793–802 (1995).
25. Samuel, A. D. T. & Berg, H. C. Torque-generating units of the bacterial flagellar motor step independently. *Biophys. J.* **71,** 918–923 (1996).
26. Leibler, S. & Huse, D. A. Porters versus rowers: a unified stochastic model of motor proteins. *J. Cell Biol.* **121,** 1357–1368 (1993).
27. Peskin, C. & Oster, G. Coordinated hydrolysis explains the mechanical behavior of kinesin. *Biophys. J.* **68,** 202s–211s (1995).
28. Duke, T. & Leibler, S. Motor protein mechanics: a stochastic model with minimal mechanochemical coupling. *Biophys. J.* **71,** 1235–1247 (1996).
29. Derényi, I. & Vicsek, T. The kinesin walk: a dynamic model with elastically coupled heads. *Proc. Natl Acad. Sci. USA* **93,** 6775–6779 (1996).
30. Astumian, R. D. Thermodynamics and kinetics of a brownian motor. *Science* **276,** 917–922 (1997).
31. Higuchi, H. & Yanagida, T. Force generation and detachment of single kinesin molecules activated by laser photolysis of caged ATP and ADP. *Cell Struct. Funct.* **23,** suppl., 198 (1998).
32. Coppin, C. M., Finer, J. T., Spudich, J. A. & Vale, R. D. Detection of sub-8-nm movements of kinesin by high-resolution optical-trap microscopy. *Proc. Natl Acad. Sci. USA* **93,** 1913–1917 (1996).

Acknowledgements. We thank Y. Inoue, M. Nishiyama, L. Satterwhite and M. Wang for discussions; J. de Georgis for squid dissection; and D. Peoples for machining. This work was supported by grants to S.M.B. from the NIGMS, NSF and W. M. Keck Foundation, predoctoral fellowships to M.J.S. to the American Heart Association, the Charlotte Elizabeth Proctor Fund, and the Program in Mathematics and Molecular Biology Burroughs Wellcome Fund, and a postdoctoral fellowship to K.V. from the Burroughs Wellcome Fund of the Life Sciences Research Foundation.

Correspondence and requests for materials should be addressed to M.J.S. (e-mail: schnitzer@physics.bell-labs.com).